EFFECT OF PYRITE TYPE ON THE ELECTROCHEMISTRY OF CHALCOPYRITE/PYRITE INTERACTIONS

Elizaveta Forbes[1]*, Leanne Smith, Mikko Vepsalainen*

CSIRO Mineral Resources, Clayton, VIC 3168, Australia

Pyrite is the most common sulphide gangue mineral occurring in base metal sulphide ores around the world. Pyrite is known to galvanically interact with valuable minerals such as chalcopyrite, altering their electrochemical and flotation behaviour. Different types of pyrite are known to vary in texture, chemical composition and electrochemical activity. However, the effect that these differences have on the degree of pyrite interaction with chalcopyrite are not well studied. This work examines two distinct types of pyrite from different deposits that have a similar chemical composition, but vary greatly in texture. It investigates the way in which these pyrites interact with chalcopyrite surfaces, affected both its electrochemical behaviour and floatability. The two pyrites were found to have similar chemical compositions and crystal lattice characteristics. Despite these similarities, the two pyrite types displayed clear differences in: surface texture, electrochemical properties (both open circuit potential and EIS), and flotation response in the presence of chalcopyrite.

[1] Corresponding Author

1 INTRODUCTION

Pyrite (FeS_2) is one of the most commonly occurring metal sulphide minerals, and its presence is ubiquitous in ores processed in the base metal sulphide industry. In some cases (such as the PGM and gold processing operations), the recovery of pyrite is desirable due to factors such as gold substitution into the pyrite lattice and close association with finely grained PGM bearing minerals. However, in the vast majority of cases, pyrite is seen as an undesirable gangue species.

Pyrite is highly floatable and readily enters the flotation concentrates, diluting the grade of valuable products. In addition, it is well known pyrite interacts with other base metal sulphide minerals, such as chalcopyrite. Such interactions are thought to boost pyrite floatability due to copper activation, while depressing chalcopyrite through galvanic passivation (Ekmekçi and Demirel, 1997; Guy and Trahar, 1985; Hu et al., 2009; Owusu et al., 2014; Trahar et al., 1994).

Recently, anecdotal reports from industrial mining operations seem to suggest that pyrites from different deposits are characterised by distinctly different flotation behaviour. Furthermore, it has been demonstrated that small variations in pyrite composition can account for significant differences in pyrite mineral characteristics, specifically, its chemical reactivity and its electrochemical properties (Abraitis et al., 2004; Xian et al., 2015). The electrochemistry of base metal sulphide surfaces is known to have a strong effect on the mineral surface hydrophobicity through the formation of hydrophobic oxidation products on mineral surfaces (Guy and Trahar, 1985; Trahar et al., 1994; Woods, 2003). It is therefore expected that strong variations within pyrite properties are likely to have consequences with regards to the flotation response of both pyrite and other base metal sulphide minerals that it comes into contact with during the flotation process. However, very few studies exist on the topic.

This work forms part of a larger study to determine the fundamental electrochemical drivers behind the effective removal of arsenic bearing minerals from base metal rich ores. Within such ore bodies, minerals such as enargite and tennantite are known to coexist with both chalcopyrite and pyrite. This paper focuses on the effect that differences in pyrite type have on surface properties and subsequent flotation characteristics of chalcopyrite. The next stage of the study would then involve evaluating these effects for both enargite and tennantite surfaces.

The objective of this paper is to study two distinctly different types of pyrite and their behaviour in the presence of chalcopyrite. The properties of the three minerals (two types of pyrite and one type of chalcopyrite) are evaluated using electrochemical, analytical and microscopy techniques. These are then compared to flotation performance.

2 EXPERIMENTAL DETAILS

2.1 Materials

Two types of pyrite were used in this study:

- Renison pyrite, sourced from Australia
- Huanzala pyrite, sourced from Peru

Initially, the study screened four different pyrite types and found that they fell into two activity categories as evidenced by their open circuit potential (see section 3.2). A single mineral from each group was selected for both clarity and efficiency purposes.

The chalcopyrite used in this study was sourced from Mt Lyell in Australia. All samples were also mounted in conjunction with a sample of enargite as part of a larger study, however the results pertaining to enargite will not be presented here.

Each mineral particle was fitted with a copper cable using conductive silver epoxy, as shown in Figure 1. The three mineral particles were then mounted in a single epoxy resin block to enable simultaneous measurement. The surface areas of each mineral particle were estimated using image analysis, with the results presented in

Table 1. Prior to each electrochemical measurement, the samples were freshly polished on first 1200 calibre grit paper, followed by 6 micron grit paper in the presence of the test solution. This technique allowed for a fresh mineral surface to be generated for each test using the same sample.

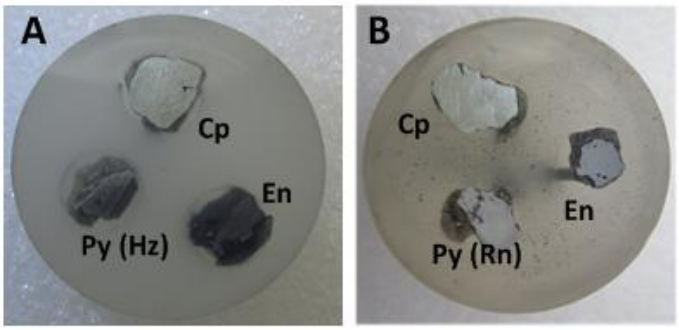


Figure 1 – Mineral electrodes used in this study

Table 1 – Mineral electrode surface areas

Mineral Type	Surface Area (cm^2)
Chalcopyrite (Electrode A)	0.37
Chalcopyrite (Electrode B)	0.46
Huanzala Pyrite	0.13
Renison Pyrite	0.27

2.2 Electrochemical Measurements

All electrochemical measurements were performed using the BioLogic M470 instrument in DC mode. The measurements were performed using the Standard Calomel Electrode as a reference, and Pt wire as a Counter Electrode. All measurements were performed in a solution of 10^{-2} M NaCl, adjusted to pH 10 using laboratory grade NaOH.

2.3 Equilibrium Open Circuit Potential Measurements

Equilibrium open circuit potentials (OCP) of each electrode and electrode couples were measured for 30 minutes. The circuit potentials for the last 10 minutes were averaged to calculate the equilibrium OCP for each condition. OCP measurements for each condition were repeated in triplicate. The average OCP values for each condition were then calculated, along with the corresponding 95% confidence limit of the mean values.

Please note that throughout this paper, all electrochemical potential values quoted in millivolts vs. Standard Hydrogen Electrode (SHE), but for the sake of brevity will be referred to as simply millivolts (mV).

2.4 Electrochemical Impedance Spectroscopy (EIS) Measurements

The impedance (Z) measurements were made as a function of frequency (f), in the range between 100 kHz and 0.1 Hz. In each case, the samples were first conditioned for 900 s at the potential corresponding to the previously determined mean OCP value for the specific test condition. The conditioning potential value was then further maintained for the duration of the measurement. Under these conditions, the impedance of mineral surfaces corresponded to the natural degree of oxidation of these surfaces within the chemical conditions imposed by the aqueous solution medium.

The tests for each condition were replicated between 3 and 6 times depending on the spread of the data. The real and imaginary components of Z(f) (Z' and Z" respectively) were plotted against one another in the form of a Nyquist plot. The resulting data sets were analysed using Bio-Logic EC-Lab V11 software to determine the equivalent circuit parameters. The average values of the resulting circuit parameters for each test condition were then calculated, along with the corresponding 95% confidence limit of the average values.

2.5 Equivalent circuit modelling

There are a great number of different types of circuit equivalents that can be used to ensure a good fit with the experimental data (Mendiratta, 2000). However, due to the simplified nature of the experimental setup, a very basic equivalent circuit diagram was used for modelling purposes, where the three circuit parameters corresponded to the physical phenomena involved in mineral oxidation.

The oxidation process involves the transfer of an electron from the surrounding solution to the mineral surface, where it can take part in a chemical reaction with that surface. According to DLVO theory (Derjaguin and Landau, 1941; Verwey and Overbeek, 1948), the electron would need to first pass through the bulk solution, followed by the double layer surrounding the surface, finally reacting with the surface itself (Figure 3).

Therefore, the three circuit parameters that were deemed to correspond to this physical system were: electrolyte resistance (R_U), double layer capacitance (C_{DL}) and resistance to surface electron transfer (R_{ET}). These circuit

parameters would then correspond to the following equivalent circuit model (shown in Figure 2), with the associated mathematical model for calculating the circuit parameter values shown in Equation 1. The equation corresponding to the chosen circuit model and its fit of the raw impedance data was provided by the fitting module of the EC-Lab software by Bio-Logic.

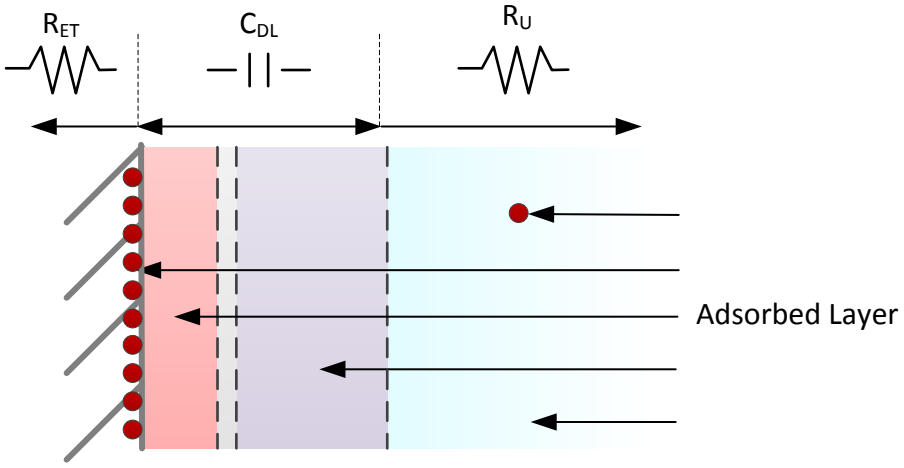


Figure 3 – Circuit equivalents for electron transfer through the electrical double layer to the mineral surface

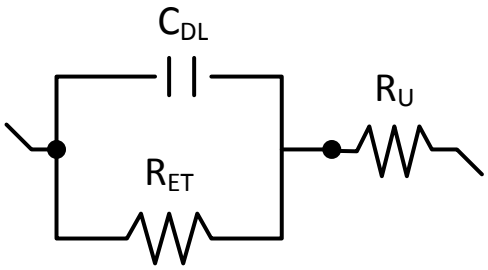


Figure 2 – Equivalent circuit model

$$Z(f) = R_U + \frac{R_U}{R_{ET} \cdot C_{DL} \cdot (i\pi f)^{\alpha} + 1} \qquad \text{Eq. 1}$$

In this simplified system, the solution conditions were kept constant. Therefore the R_U values are expected to remain constant within the bounds of experimental error. The properties of the electrical double layer depend on two parameters: the ionic strength of the bulk solution and the electrochemical potential (or charge) of the surface itself. Since the electrolyte solution was kept consistent throughout the experiments, the differences in the calculated double layer capacitance (C_{DL}) values are expected to be due to the differences in the mineral surface charge.

Finally, the magnitude of the resistance to the surface electron transfer (R_{ET}) then corresponds to the degree of activity of the mineral surface and its resistance to oxidation. A high R_{ET} would then correspond to a relatively passive surface, not prone to oxidation. On the other hand, a low R_{ET} value would correspond to an active surface that readily oxidises.

2.6 Flotation Tests

2.6.1 Mineral samples

Pyrite (Py) and chalcopyrite (Cp) samples were separated from high grade ore by hand picking. The upgraded portion was then stage crushed in a laboratory jaw crusher to pass 10 mesh (1.65 mm) and screened at 65 mesh (212 μm) to remove fines. High quality quartz obtained locally and prepared in a similar manner to the pyrite and chalcopyrite samples was used as the gangue mineral in all flotation tests.

Charges of 50 g (for single mineral tests) and 25 g (for multiple mineral tests) were riffled from each of the bulk samples for flotation testing. It is known that metal hydroxides produced from oxidation of the mineral surfaces interfere with the floatability of sulphides. To eliminate the possible effects of any hydroxides on the self-induced floatability of chalcopyrite and pyrite in this flotation study, the sulphide mineral charge was washed with 50 ml of a 1% solution of the tri-sodium salt of ethylene diamine tetraacetic acid (EDTA) and rinsed 3 times with distilled water before grinding to remove any such oxidation products.

2.6.2 Reagents

All tests were conducted in the absence of collector. The EDTA used was laboratory grade. The frother used was a commercial polypropylene glycol prepared as a 0.25% w/v solution. Frother solution was added continually at a rate of 5 mg min^{-1} from one minute prior to flotation to maintain an active froth. Dilute sodium hydroxide solutions were used to adjust the pH. All water was distilled and the flotation gas was high purity synthetic air used at a flow rate of 8 dm^3 min^{-1}.

2.6.3 Grinding

For each flotation test, 50 g of sulphide mineral (either 50 g of one mineral only in single mineral tests or 25 g of chalcopyrite and 25 g of the pyrite of choice in mixed mineral tests) and 450 g of quartz were ground for 20 minutes in a stainless steel ball mill at a solid-liquid ratio of 2:1 (i.e. 67% solids by weight). A stainless steel rather than iron mill was used to avoid the reducing conditions of closed iron mills.

2.6.4 Flotation Procedure

The flotation tests were performed in a 3 L modified Denver cell (Guy, 1992) in which the impeller was driven from below to allow the whole surface of the froth to be scraped with a paddle at a constant depth and at constant time intervals. The cell was fitted with a rubber diaphragm, sight tube and electronic sensor for automatic detection and control of the pulp level.

The ground pulp was put in the flotation cell, the pH adjusted to pH 10 and the pulp level made up to the set level. The pulp was then aerated for 5 minutes to ensure the pulp potential was at the air set potential (approximately 280 mV). The pulp potential and pH were monitored continuously throughout the tests. Potentials were measured with a polished platinum flag electrode using a Ag/AgCl reference and converted to the standard hydrogen electrode (SHE) scale by the addition of 0.2 V. A combination glass/red rod pH electrode was used to monitor the pH.

One minute before flotation, the air was turned off and frother addition commenced. Concentrates were taken after 0.5, 1, 2, 4 and 8 minutes. The froth was scraped every 2 s for the first minute of flotation and every 5 s thereafter. Flotation products were weighed both wet (to allow calculation of water recoveries) and dry, and were prepared for analysis in a standard manner.

2.6.5 Analysis of products

Products were assayed for copper, iron and sulphur by inductively coupled plasma (ICP) optical emission spectrometry. The flotation behaviour of chalcopyrite in mixed mineral tests was determined from the copper assays and the flotation behaviour of pyrite was calculated from the sulphur assays with allowance for the sulphur present as chalcopyrite.

3 RESULTS

3.1 Mineral Composition

3.1.1 Assay Analysis

A representative sample of each mineral was assayed to determine its respective copper and iron content. A summary of the results is presented in Table 2. The results show that both Huanzala and Renison pyrites contained similar quantities of impurities. The chemical composition of both pyrite is also very similar, displaying a S:Fe ratio of 1.13 and 1.14 for Huanzala and Renison pyrites respectively, indicating both pyrite types fall into the n-pyrite category (S:Fe ratio of < 2). This make them similar to the pyrite samples tested in other studies ((Abraitis et al., 2004; Doyle and Mirza, 1996).

Table 2 – Elemental assay analysis of the mineral samples

Composition	Huanzala Py	Renison Py	Mt Lyell Cp
Cu	-	-	34.3%
Fe	45.1%	44.6%	30.3%
S	51.5%	50.6%	34.9%
Other	3.4	4.8%	0.5%
TOTAL	100.0%	100.0%	100.0%

3.1.2 QXRD Analysis

A more detailed analysis of the minerals in question was performed using quantitative x-ray diffraction (QXRD), with the results are presented in Table 3. The QXRD analysis revealed that Renison pyrite contained a significantly higher quantity of quartz and cristobaite within its matrix. Since both of these minerals are electrochemically inactive, they are not likely to significantly contribute to the overall electrochemical properties of Renison pyrite.

Table 3 – QXRD analysis of the mineral samples

Composition	Huanzala Py	Renison Py	Mt Lyell Cp
Pyrite	97.9%	91.0%	-
Quarz/Cristobalite	1.0%	8.0%	5.9%
Mica	1.1%	1.0%	1.2%
Kaolinite	-	-	0.9%
Chalcopyrite	-	-	90.9%
Covellite	-	-	1.1%
TOTAL	100.0%	100.0%	100.0%

In addition to composition analysis of the three mineral samples, a Reitveld analysis was performed to determine their crystal lattice characteristics. Table 4 presents a summary of the lattice characteristics, specifically crystal orientation and a lattice spacing parameter. In the case of crystal orientation, a perfect orientation (a single crystal) will have a value of 0, while an amorphous substance will return a value of 1. The results show that all three minerals have similar orientation values, with Renison pyrite displaying a slightly better orientated structure.

Table 4 – Crystal lattice characteristics (Reitveld analysis) of the mineral samples

Lattice Characteristics	Huanzala Py	Renison Py	Mt Lyell Cp
Chalcopyrite (112) Orientation	-	-	0.77
Pyrite (002) Orientation	0.77	0.75	-
Measured Lattice Parameter (Å)	5.418	5.418	5.289
Ideal Lattice Parameter (Å)	5.418	5.418	5.289

Table 4 also presents values for the crystal lattice spacing parameter for all three minerals, alongside the ideal crystal lattice spacing parameter expected for these mineral types. In all three cases the lattice parameters perfectly match those for pyrite and chalcopyrite, respectively. The lattice parameters for Huanzala and Renison pyrites were found to be identical.

3.1.3 SEM Analysis

The surfaces of the two pyrites were analysed using SEM imaging, with the results presented in Figure 5. The figure shows both Huanzala (A) and Renison (B) pyrite surfaces at two magnification levels. The figure clearly indicates that the surface of Huanzala pyrite is extremely smooth and free of features. On the other hand, Renison pyrite displays a rough and pitted texture. Both pyrite samples underwent an identical sample preparation procedure, eliminating the possibility that the imperfections seen on the surface of Renison pyrite are due to sample polishing.

A close-up view of the Renison pyrite surface is presented in Figure 4. The image demonstrates that the pitting effect is non-random, displaying prominent 90° angle striations throughout. This corresponds well with the fact that pyrite is a cubic mineral and is expected to display 90° cleavage. This suggests that the observed pitting is somehow related to the inherent crystal structure of Renison pyrite. However, the reasons for this are unclear, as other analytical techniques have shown the two types of pyrite to be chemically similar.

The available literature that describes variations between pyrite types tends to indicate that the differences originate with micro-variations within the pyrite chemical structure, specifically the presence of small quantities of arsenic (Abraitis et al., 2004; Doyle and Mirza, 1996). On the other hand, Xian et al. (2015) found that although different types of pyrite can have similar stoichiometry and chemical composition, they may differ in spatial symmetry, which accounts for differences in both oxidation and flotation behaviour. In that study the spatial symmetry differences were determined using x-ray photoelectron spectroscopy (XPS), rather than QXRD. It may be necessary to employ a similar technique to the analysis of both Renison and Huanzala pyrites to determine where the structural differences originate from.

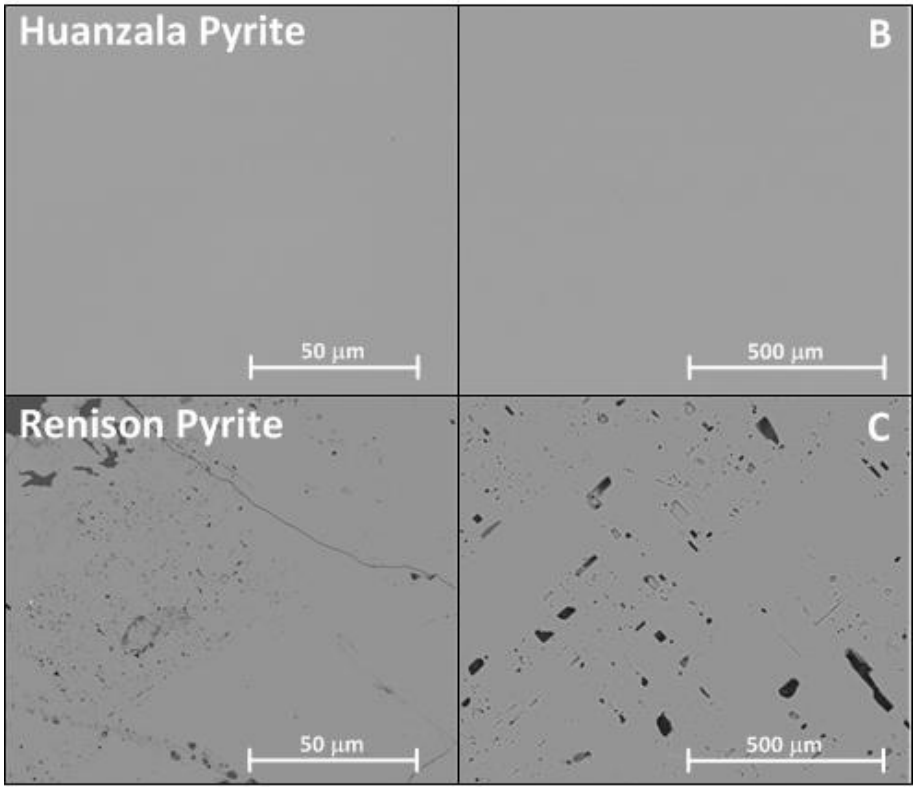


Figure 5 – SEM analysis of A) Huanzala and B) Renison pyrite surfaces at different levels of magnification

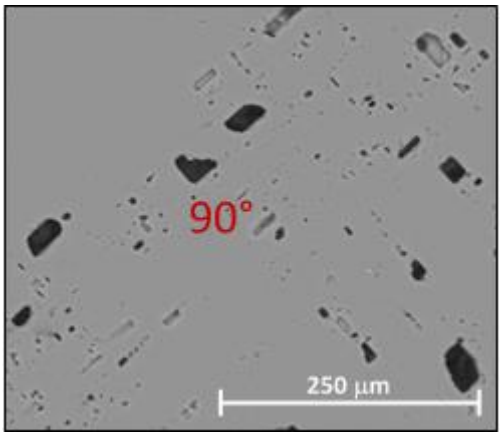


Figure 4 – Surface pitting and striations at 90° angles on the surface of Renison pyrite

3.2 Open Circuit Potential Measurements

The effect of mineral potential on the self-induced flotation of sulphide minerals has been well established (Ekmekçi and Demirel, 1997; Guy and Trahar, 1985; Woods, 2003). The natural or applied electrochemical potential causes the surfaces of sulphide minerals to oxidise. The oxidation process typically results in the formation of highly hydrophobic elemental sulphur species on the mineral surfaces, rendering them naturally

floatable. Different minerals oxidise at different electrochemical potential levels, something that is explored to obtain selective flotation and/or depression of minerals (Heyes and Trahar, 1979; Luttrell and Yoon, 1984; Owusu et al., 2014; Richardson et al., 1984).

Different mineral types also have a tendency to have a specific natural or rest potential under specific chemical conditions (such as pH). Such open circuit potential (OCP) values were measured for chalcopyrite, Renison pyrite and Huanzala pyrite electrodes at pH 10. The OCP values for electron pairs were similarly measured, with the results presented in Figure 6.

The results show that the open circuit potential (OCP) of chalcopyrite was measured at 200 mV whereas the OCP of the pyrite samples was significantly higher, at 300 and 600 mV for the Huanzala and Renison pyrite samples respectively. The difference in the OCP values between the two pyrite types is highly significant. Doyle and Mirza (1996) tested the rest potentials of 12 different types of n-pyrite and found very little variation between them, with the measurements falling in the range between 558 – 699 mV, with the average resting at 647 mV. While the OCP measurements for Renison pyrite are consistent with these findings, the values obtained for Huanzala pyrite represent a significant departure, indicating that the two pyrite types have significantly different oxidation properties, despite the similarities in their chemical and crystal structures (see Section 3.1).

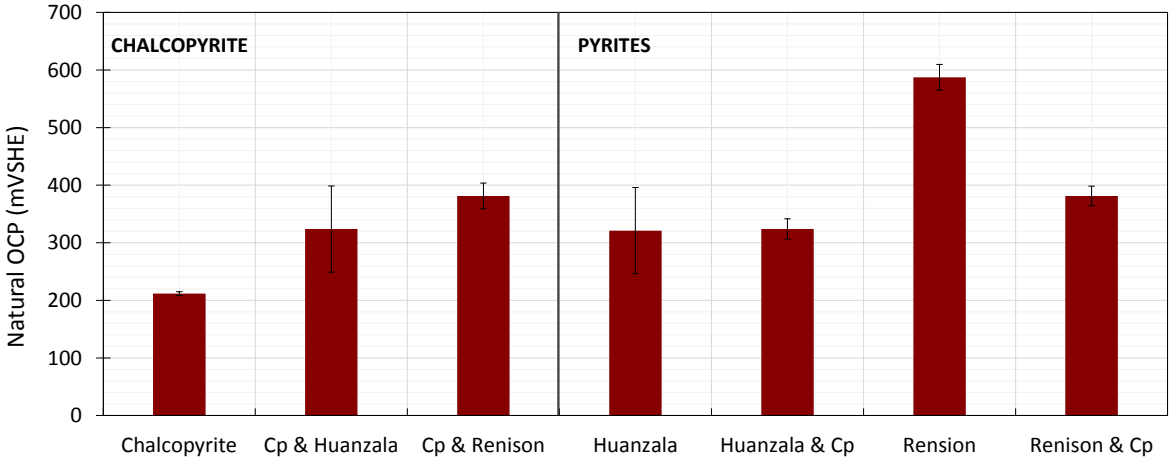


Figure 6 – Equilibrium open circuit potential measurements for pure minerals and mineral couples, error bars represent the 95% confidence interval of the mean

The measured potentials of each chalcopyrite and pyrite galvanic couple were similar, in the range of 300-400 mV. Within such a pairing, pyrite is the nobler electrode (characterised by the higher rest potential) and will act as a cathode in the galvanic interaction, whereas chalcopyrite will act as the anode. Such a galvanic interaction would then enhance the oxidation rate on the chalcopyrite surface, forming elemental sulphur and CuS species, whereas the cathodic reaction on the pyrite surfaces would reduce ferric hydroxide to ferrous hydroxide (Ekmekçi and Demirel, 1997).

It is expected that the significantly higher potential of Renison pyrite compared to Huanzala pyrite would enhance the galvanic interaction. However, the electrode reactions of the galvanic couple are also influenced by the surface area ratios of minerals, which were not same in the Cp-Huanzala and Cp-Renison pairs. The Cp:Py surface area ratios for Cp-Huanzala and Cp-Renison pairs were 2.84 and 1.71, respectively (see Table 1), which means that the influence of Renison pyrite on the galvanic coupling was significantly reduced compared to that

of Huanzala pyrite. This means that although the final OCP values of the two galvanic pairings were similar, Huanzala pyrite had a significantly weaker influence on the galvanic chalcopyrite/pyrite pairing than the Renison pyrite.

It is also important to mention that the apparent measured electric surface areas presented in Table 1 do not necessarily represent the overall active surface areas of the electrodes. The SEM images presented in figures 4 and 5 demonstrated that the surface of Renison pyrite contained microscopic pitting, while that of Huanzala pyrite was mirror smooth. The difference in texture is bound to have a contribution towards the overall available mineral surface area. However, the magnitude of this contribution has not been measured and hence cannot be commented upon further.

3.3 Electrochemical Impedance Spectroscopy (EIS) Measurements

Once the open circuit potentials of the three minerals and their pairings have been established, the matching EIS measurements were performed. It is important to note that prior to and during the EIS measurements, the electrical potential was maintained at the corresponding OCP measurements presented in Figure 6.

For each test condition, the real (Z') and imaginary (Z") components of the impedance spectra were plotted on a Nyquist diagram and fitted with the equivalent circuit model, as shown in Figure 7. The model takes the form of a semicircle, where the values of the uncompensated background electrolyte resistance (R_U) and resistance to electron transfer (R_{ET}) can be calculated from the two x intercept values. The average R_{ET} values obtained for the minerals and mineral couples are presented in Figure 8.

Figure 7 demonstrates that the impedance data measured for this system of electrodes corresponds well to similar measurements made in such systems available in literature (Hu et al., 2009). It also shows that the circuit model (Equation 1) is a reasonably good fit for the experimental data over the majority of the measured range.

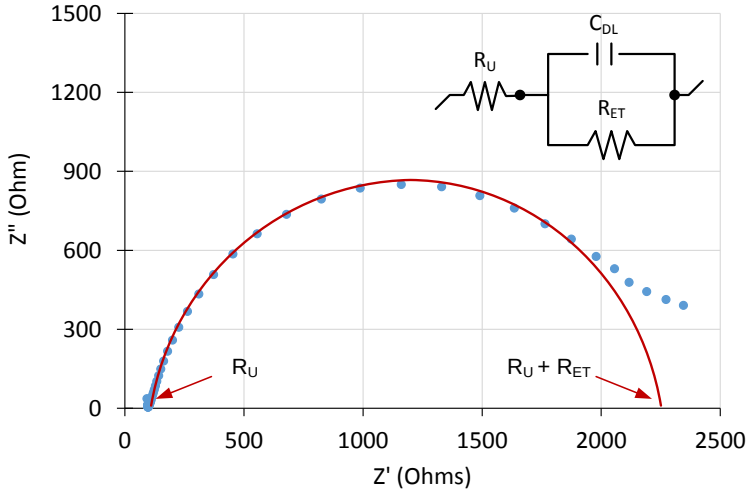


Figure 7 – Example of a Nyquist diagram (data for a test using Renison pyrite, at a potential of 587 mV) being fitted with the equivalent circuit model

A summary of all the calculated electron transfer resistance (R_{ET}) values is presented in Figure 8. It must be noted that a significant amount of variation was detected between repeated measurements for the same conditions, which are reflected in the 95% confidence interval error bars. Such a high degree of variation likely results from the fact that the samples were freshly polished before each measurement. The act of polishing has previously been blamed for similar variations in other studies (Mendiratta, 2000). However, despite the high degree of variation, the differences in the R_{ET} values can still be considered significant.

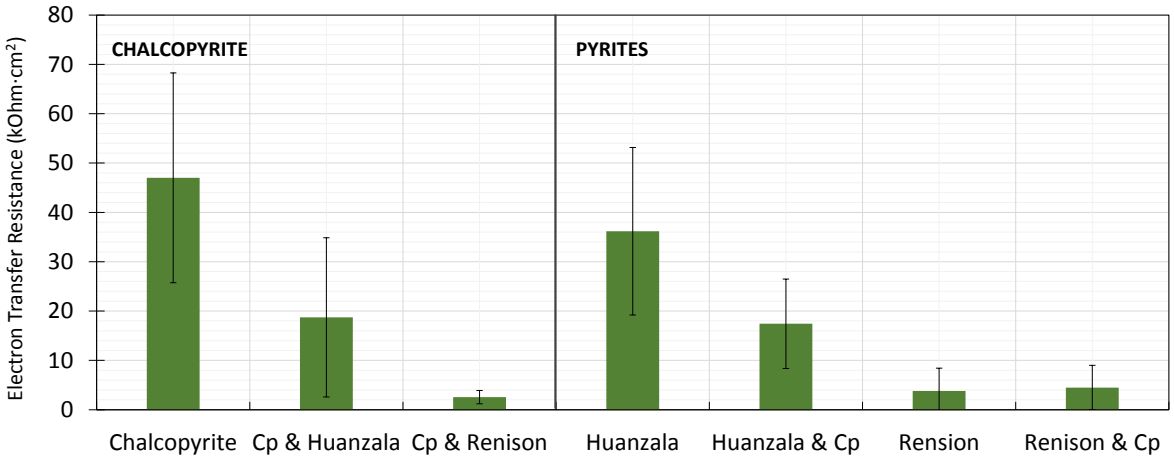


Figure 8 – Electron transfer resistance (R_{ET}) values derived from Nyquist plots for pure minerals and mineral couples, error bars represent the 95% confidence interval of the mean

According to electrochemical impedance spectroscopy (EIS) results the galvanic interaction between the chalcopyrite and pyrite samples significantly suppressed the charge transfer resistance (R_{ET}) of the chalcopyrite electrodes. This indicates an enhanced reaction rate on the surface which in this system would be the oxidation of the mineral according to Equation 2 (Gardner and Woods, 1979):

$$CuFeS_2 + 3H_2O \leftrightarrow CuS + Fe(OH)_3 + S^0 + 3H^+ + 3e^- \quad \text{Eq. 2}$$

Further oxidation of the CuS may occur according to Equation 3:

$$CuS + 2H_2O \leftrightarrow Cu(OH)_2 + S^0 + 2H^+ + 2e^- \quad \text{Eq. 3}$$

Renison pyrite had a significantly stronger effect on the chalcopyrite charge transfer resistance value than Huanzala pyrite. The results are supported by the OCP values, according to which Renison pyrite is nobler and had stronger galvanic effect with the chalcopyrite. The charge transfer resistance of Huanzala pyrite decreased when it was in contact with the chalcopyrite sample whereas the charge transfer resistance of Renison pyrite was not significantly affected.

3.4 Flotation Measurements

The results of the flotation tests are shown in Figures 9 and 10 in the form of recovery-time plots. From the curves for the single sulphide mineral tests in the absence of collector, it can be seen that chalcopyrite is strongly floatable at pH 10 while both pyrites are poorly floatable. This in line with other published results (Ekmekçi and Demirel, 1997; Trahar et al., 1994) of the flotation of chalcopyrite and pyrite in the absence of collectors. The strong flotation of chalcopyrite in the absence of collector in alkaline conditions is thought to be due to the

formation of elemental sulphur due to oxidation of the chalcopyrite surface, according Equations 2 and 3. The oxidation of pyrite can be interpreted in terms of the following reactions (Hamilton and Woods, 1981):

$$FeS_2 + 3H_2O \rightarrow Fe(OH)_3 + 2S^\circ + 3H^+ + 3e^- \quad \text{Eq. 4}$$

$$FeS_2 + 11H_2O \rightarrow Fe(OH)_3 + 2SO_4^{2-} + 19H^+ + 15e^- \quad \text{Eq. 5}$$

The poor flotation of pyrite in the absence of collector in alkaline conditions is thought to be due to the dominance of Equation 5 over Equation 4 (Heyes and Trahar, 1984), where sulphate species are begin formed on pyrite surfaces instead of elemental sulphur. According to the open circuit potential results (Figure 6), the potential of chalcopyrite increases when it is in galvanic contact with pyrite. In this system pyrite would be the cathode of the cell and chalcopyrite the anode. According to the impedance spectroscopy results the electron transfer resistance (R_{ET}) of chalcopyrite significantly decreases in the presence of the galvanic contact with pyrite. This would indicate a faster reaction rate on the chalcopyrite surface and hence Equations 2 and 3 would be pushed further to the right, producing higher concentrations of metal hydroxides.

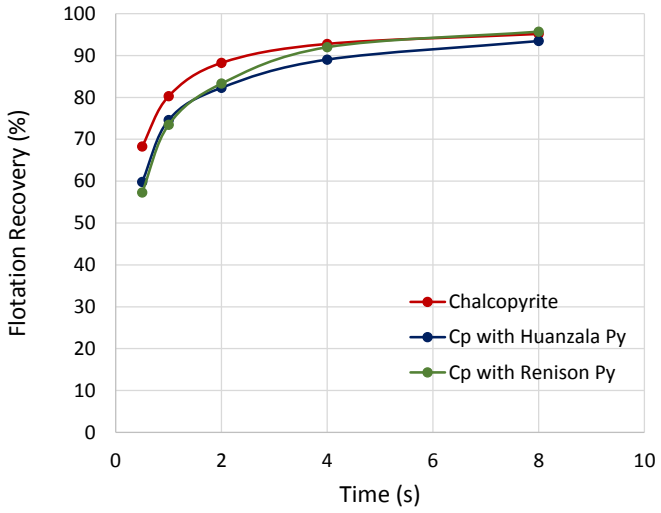


Figure 9 – Flotation recoveries for chalcopyrite, both in the presence and absence of the two pyrite types, performed at pH 10, at an air set potential of ≈ 280 mV_{SHE}

The strong floatability of chalcopyrite in the absence of collector has been shown to be diminished by the presence of metal hydroxides (Guy and Trahar, 1985; Woods, 2003). Therefore it was expected that the floatability of chalcopyrite from the chalcopyrite/pyrite/quartz mixtures may be diminished as a result of increased oxidation. However, chalcopyrite flotation in the current study (Figure 9) was not significantly affected by the presence of pyrite. There was a small decrease in the rate of chalcopyrite flotation in the presence of pyrite but overall chalcopyrite recoveries were not significantly different.

Ekmekçi and Demirel (1997) found that chalcopyrite floatability significantly decreaseed with an increasing Py:Cp ratio in the flotation pulp. However, at similar Cp/Py/Q proportions as in these tests, the effect of the presence of pyrite on chalcopyrite flotation was minimal.

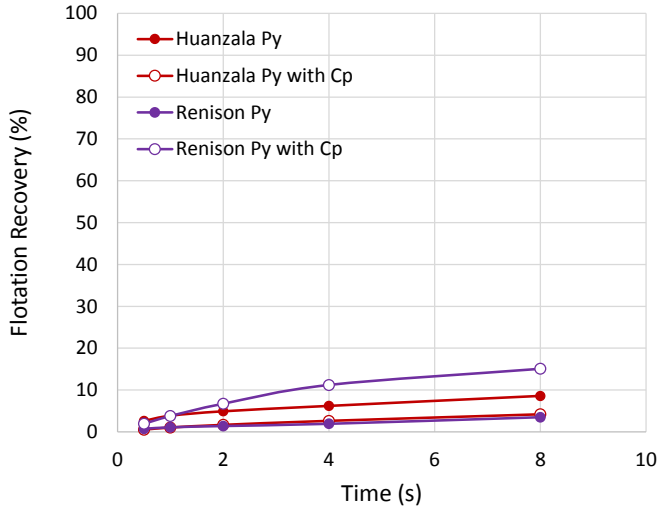


Figure 10- Flotation recoveries for Huanzala and Renison pyrites, both in the presence and absence of chalcopyrite, performed at pH 10, at an air set potential of ≈ 280 mV_{SHE}

Pyrite flotation in the presence of chalcopyrite was still poor. The floatability of Huanzala pyrite decreased slightly in the presence of chalcopyrite but the difference was so small that it fitted well within the typical level of experimental error (≈ 5%) due to inconsistencies with water recovery or feed distribution. The floatability of Renison pyrite, however, increased in the presence of chalcopyrite from 4% to 13% which is probably more than could be accounted for by changes in water recovery and/or feed distribution. Due to the significantly higher potential of Renison pyrite, the galvanic interaction with the chalcopyrite would be expected to be enhanced compared to Huanzala pyrite. Ekmekçi and Demirel (1997) also found that the flotation of pyrite in the absence of collector increased in the presence of chalcopyrite.

Ekmekçi and Demirel (1997) suggested two different mechanisms for the increased flotation of pyrite: (a) elemental sulphur or metal-deficient sulphur generated by the pyrite itself; or (b) copper activation of the pyrite. These mechanisms would take place as a result of the galvanic interaction between the two sulphide minerals. Normally pyrite oxidises according to Equation 5 producing sulphate ions. The first mechanism would require that in the presence of chalcopyrite, the oxidation of pyrite would be modified in such a manner as to make Equation 4 more likely.

Copper activation of pyrite was discounted by Trahar et al. (1994), as they were unable to increase the self-induced flotability of pyrite by the addition of copper ions. Trahar et al. (1994) did detail circumstances under which pyrite could be shown to exhibit self-induced flotation by the transfer of a sulphur entity from a mineral such as chalcopyrite or galena to the pyrite. Such behaviour may be governed by increased sulphur production through increased oxidation of the chalcopyrite as a result of the galvanic interaction between chalcopyrite and pyrite.

The galvanic interaction would also be influenced by the available surface area of the sulphides, so changes in the proportions of sulphides in the mixtures may lead to higher pyrite recoveries, as observed by Ekmekçi and Demirel (1997). At this point, it is once again important to note that the pitting and striations on the surface of Renison pyrite (as illustrated in Figure 4) may serve to cause the surface area of Renison pyrite particles to be greater than those of Huanzala pyrite, at the same particle size distribution.

4 CONCLUSIONS

From the information presented in this paper, the following conclusions can be drawn:

- The two pyrites examined in this study (Renison and Huanzala pyrite) were found to have similar chemical compositions and crystal lattice characteristics. Despite these similarities, the two pyrite types displayed clear differences in: surface texture, electrochemical properties (both open circuit potential and EIS), and flotation response in the presence of chalcopyrite.

- The open circuit potential and EIS measurements indicated that Renison pyrite surfaces are more affected by the galvanic interaction with chalcopyrite than Huanzala pyrite surfaces, which remain largely unchanged.

- This was confirmed by the fact that the floatability of Renison pyrite improved in the presence of chalcopyrite, while that of Huanzala pyrite remained unchanged. The increase in Renison pyrite floatability can be attributed to a greater degree of surface oxidation, which may lead to the formation of elemental sulphur species on Renison pyrite surfaces.

- The galvanic pairing of chalcopyrite with Renison pyrite had a significantly stronger effect on the open circuit potential and electrochemical impedance of chalcopyrite than Huanzala pyrite.

- The pairing with neither one of the pyrite types caused a significant shift in the floatability of chalcopyrite. Further work is necessary to investigate this effect.

- The cause of the differences between the two pyrite types remains unclear and further work is required to establish it. One of the potential areas of focus is the presence of 90° striations on the surface of Renison pyrite. Such textural features may potentially be indicative of two things: a significantly larger surface area per unit mass of mineral at the same particle size distribution, and/or a significant variation in the Renison pyrite crystal spacing/configuration that was not picked up by QXRD measurements. Future work may need to employ a more sensitive technique, such as X-ray photoelectron spectroscopy (XPS) to determine the nature of these differences.

5 ACKNOWLEDGMENTS

The authors would like to acknowledge the help and contribution of Mathew Glenn (Scanning Electron Microscopy); Nathan Webster (Quantitative X-Ray Diffraction), Cheryl McHugh (Inductively Coupled Plasma Mass Spectrometry), and Luda Malishev for laboratory assistance.

6 REFERENCES

Abraitis, P.K., Pattrick, R.A.D., Vaughan, D.J., Variations in the compositional, textural and electrical properties of natural pyrite: a review. International Journal of Mineral Processing, 2004, **74(1–4)**, 41-59.

Derjaguin, B.V., Landau, L., Theory of stability of strongly charged lyophobic sols and the adhesion of strongly charged particles in solution of electrolytes. Acta Physiochim, 1941, **14**, 633 - 662.

Doyle, F.M., Mirza, A.H., 1996. Electrochemical oxidation of pyrite samples with known composition and electrical properties, In *Electrochemical Proceedings* pp. 203 - 214.

Ekmekçi, Z., Demirel, H., Effects of galvanic interaction on collectorless flotation behaviour of chalcopyrite and pyrite. International Journal of Mineral Processing, 1997, **52(1)**, 31-48.

Gardner, J.R., Woods, R., An electrochemical investigation of the natural flotability of chalcopyrite. International Journal of Mineral Processing, 1979, **6(1)**, 1-16.

Guy, P.G., Trahar, W.J., 1985. The Effects of Oxidation and Minreal Interaction on Sulfide Flotaiton, In *Flotation of Sulfide Minerals*, ed. Forrsberg, E. Elsevier, pp. 63 - 71.

Guy, P.J., 1992. The development of laboratory batch flotation equipment and practice at CSIRO Australia, In *AusIMM Annual Conference*. AusIMM, Melbourrne, Australia, pp. 75 - 79.

Hamilton, I.C., Woods, R., An investigation of surface oxidation of pyrite and pyrrhotite by linear potential sweep voltammetry. Journal of Electroanalytical Chemistry and Interfacial Electrochemistry, 1981, **118**, 327-343.

Heyes, G.W., Trahar, W.J., Oxidation-Reduction effects in the flotation of chalcocite and cuprite. International Journal of Mineral Processing, 1979, **6(3)**, 229-252.

Heyes, G.W., Trahar, W.J., 1984. The flotation of pyrite and pyrrhotite in the absence of conventional collectors, In *Electrochemistry in Minerals and Metal Processing*, eds. Richardson, P.E., Srinivasan, S., Woods, R., pp. 219-232.

Hu, Y., Sun, W., Wang, D., 2009. Chapter 7 - Corrosive Electrochemistry of Oxidation-Reduction of Sulfide Mienrals, In *Electrochemistry of Flotation of Sulphide Minerals*. Springer-Verlag, Berlin Heidelberg, pp. 167 - 200.

Luttrell, G.H., Yoon, R.-H., The collectorless flotation of chalcopyrite ores using sodium sulfide. International Journal of Mineral Processing, 1984, **13(4)**, 271-283.

Mendiratta, N.K., 2000. Kinetic Studies of Sulfide Mineral Oxidation and Xanthate Adsorption, In *Materials Engineering and Science*. Virginia Polytechnic Institute.

Owusu, C., Brito e Abreu, S., Skinner, W., Addai-Mensah, J., Zanin, M., The influence of pyrite content on the flotation of chalcopyrite/pyrite mixtures. Minerals Engineering, 2014, **55**, 87-95.

Richardson, P.E., Stout, J.V., Proctor, C.L., Walker, G.W., Electrochemical flotation of sulfides: Chalcocite-ethylxanthate interactions. International Journal of Mineral Processing, 1984, **12(1–3)**, 73-93.

Trahar, W.J., Senior, G.D., Shannon, L.K., Interactions between sulphide minerals — the collectorless flotation of pyrite. International Journal of Mineral Processing, 1994, **40(3)**, 287-321.

Verwey, E.J.W., Overbeek, J.T.G., *Theory of Stability of Lyophobic Solids*. 1948, Elsevier, Amsterdam.

Woods, R., Electrochemical potential controlling flotation. International Journal of Mineral Processing, 2003, **72(1)**, 151-162.

Xian, Y., Wang, Y., Wen, S., Nie, Q., Deng, J., Floatability and oxidation of pyrite with different spatial symmetry. Minerals Engineering, 2015, **72**, 94-100.